THE JOURNAL OF BIOLOGICAL CHEMISTRY VOL. 287, NO. 45, pp. 38101–38109, November 2, 2012

Avirulence Protein 3a (AVR3a) from the Potato Pathogen *Phytophthora infestans* Forms Homodimers through Its Predicted Translocation Region and Does Not Specifically Bind Phospholipids*[S]

Received for publication, June 26, 2012, and in revised form, September 10, 2012 Published, JBC Papers in Press, September 12, 2012, DOI 10.1074/jbc.M112.395129

Stephan Wawra,[a1] Mark Agacan,[b] Justin A. Boddey,[c,d] Ian Davidson,[e] Claire M. M. Gachon,[f] Matteo Zanda,[g,h] Severine Grouffaud,[a,i] Stephen C. Whisson,[j] Paul R. J. Birch,[i,j] Andy J. Porter,[k] and Pieter van West[a2]

From the [a]Aberdeen Oomycete Laboratory, College of Life Sciences and Medicine, the [e]Proteomics Facility, [h]Kosterlitz Centre for Therapeutics, and [k]Molecular and Cell Biology, Institute of Medical Sciences, University of Aberdeen, Foresterhill, Aberdeen AB25 2ZD, Scotland, United Kingdom, the [b]Proteomics Facility, College of Life Sciences, University of Dundee, Dundee DD1 5EH, Scotland, United Kingdom, the [c]Division of Infection and Immunity, The Walter and Eliza Hall Institute, and the [d]Department of Medical Biology, University of Melbourne, Parkville, Victoria 3052, Australia, the [f]Scottish Association for Marine Science, Scottish Marine Institute, Oban, Argyll PA37 1QA, Scotland, United Kingdom, the [g]Istituto di Chimica del Riconoscimento Molecolare, Consiglio Nazionale delle Ricerche, 20131 Milan, Italy, and [i]Cell and Molecular Sciences, The James Hutton Institute, and the [j]Division of Plant Sciences, College of Life Sciences, University of Dundee at JHI, Invergowrie, Dundee DD2 5DA, Scotland, United Kingdom

Background: AVR3a is a *Phytophthora infestans* effector that translocates into potato cells dependent on the N-terminal R*x*LR leader.
Results: AVR3a dimerization is inhibited by a mutation that also impairs translocation.
Conclusion: Phospholipid binding of AVR3a is probably physiologically irrelevant because only denatured protein molecules bind.
Significance: Our findings will help us to understand how oomycete R*x*LR effectors function.

The mechanism of translocation of R*x*LR effectors from plant pathogenic oomycetes into the cytoplasm of their host is currently the object of intense research activity and debate. Here, we report the biochemical and thermodynamic characterization of the *Phytophthora infestans* effector AVR3a *in vitro*. We show that the amino acids surrounding the R*x*LR leader mediate homodimerization of the protein. Dimerization was considerably attenuated by a localized mutation within the R*x*LR motif that was previously described to prevent translocation of the protein into host. Importantly, we confirm that the reported phospholipid-binding properties of AVR3a are mediated by its C-terminal effector domain, not its R*x*LR leader. However, we show that the observed phospholipid interaction is attributable to a weak association with denatured protein molecules and is therefore most likely physiologically irrelevant.

The oomycetes (or water molds) encompass many devastating pathogenic species (1, 2). Among them, *Phytophthora infestans* causes potato late blight, a disease of concern for global food security. Like all successful pathogens, oomycetes are able to evade the defense reactions of their hosts. One of their common strategies is to manipulate their host's immune system by secreting effectors that interfere with intracellular components of basal or inducible immunity (*e.g.* Refs. 3–5).

Recently, it was shown that several plant pathogenic oomycetes contain genes that encode putative secreted proteins that all contain a conserved tetrameric amino acid sequence motif: R*x*LR. This Arg-Xaa-Leu-Arg motif is found within 40 amino acids following the predicted cleavage sites of canonical signal peptides and is often followed by a Glu-Glu-Arg (EER) motif (6–8).

To date, the best characterized R*x*LR effector is AVR3a from *P. infestans* (see Scheme 1*A* for a schematic summary of the current published literature). AVR3a was originally identified as the cognate avirulence protein recognized by the cytosolic potato R3a resistance protein (9). AVR3a is a small secreted protein that is delivered into host cells by the pathogen via an unknown mechanism dependent on the N-terminal R*x*LR leader (8). *In planta* coexpression of R3a and different AVR3a truncation constructs showed that amino acids 73–147 were sufficient to trigger the R3a-mediated hypersensitive response, but the response was reduced compared with AVR3a lacking only the signal peptide (residues 1–21) or the signal peptide and the R*x*LR leader (amino acids 1–59). Furthermore, deletion of the last 16 residues abolished any recognition by R3a (10). Two isoforms of AVR3a have been identified in *P. infestans* isolates that differ by only three amino acids. Two of these changes, at

* This work was supported by the Biotechnology and Biological Sciences Research Council (BBSRC; to S. W., P. R. J. B., A. J. P., and P. v. W.), the Natural Environmental Research Council (NERC; to S. W., C. M. M. G., and P. v. W.), the University of Aberdeen (to S. G., I. D., A. J. P., M. Z., and P. v. W.), the University of Dundee (to M. A. and P. R. J. B.), the Scottish Government Rural and Environmental Science Analytical Services Division (RESAS; to S. C. W.), and The Royal Society (to P. v. W.).
[S] This article contains supplemental "Materials and Methods," Figs. S1–S10, Notes 1 and 2, Appendices 1–3, and additional references.
[1] To whom correspondence may be addressed. E-mail: s.wawra@abdn.ac.uk.
[2] To whom correspondence may be addressed. E-mail: p.vanwest@abdn.ac.uk.

positions 80 and 103, are present in the mature proteins lacking the signal peptide. AVR3a$^{(C19)K80I103}$ is referred to here as AVR3a^{KI}, and AVR3a$^{(S19)E80M103}$ is referred to as AVR3a^{EM}. Whereas AVR3a^{KI} is quite efficiently recognized by R3a, AVR3a^{EM} is weakly recognized. Thus, strains expressing only the AVR3a^{EM} isoform evade recognition by plants carrying the *R3a* resistance gene and do not induce a defensive hypersensitive response (9, 10).

AVR3a modulates the plant immune response by stabilizing the host ubiquitin E3 ligase CMPG1. By doing so, it suppresses a plant defense response against another *P. infestans* secreted protein, INF1 (5). Crucial for this biological function of AVR3a is the presence of a freely accessible C-terminal aromatic residue (Tyr-147). However, modification or deletion of Tyr-147 from the AVR3a^{KI} C terminus did not interfere with R3a recognition (5). An explanation for this observation was suggested by the recently published structural model of AVR3a. This model was based on the NMR structure of the *Phytophthora capsici* homolog, AVR3a4 and shows that the C terminus is flexible and angled away from the four-bundle helical protein core. However, no defined structural information could be obtained from the R*x*LR leader of *P. capsici* AVR3a4 to potentially shed light on the requirements for translocation, despite this region being included in the recombinant protein under study (4).

In 2010, Kale *et al.* (11) reported that R*x*LR and R*x*LR-like proteins are translocated into eukaryotic cells via an R*x*LR-dependent, pathogen-independent mechanism. In addition, the authors claimed that R*x*LR or R*x*LR-like motifs mediate translocation through binding to phosphoinositol 3-phosphate molecules exposed at the cell surface. However, this view has been recently challenged by two independent studies (4, 12). Using recombinant AVR3a from *P. infestans*, Yaeno *et al.* (4) showed that the effector domain, rather than the R*x*LR leader, binds to phospholipids (PLPs).[3] Using *in planta* expression of AVR3a effector domain point mutants (*i.e.* K85E) that did not show any PLP binding *in vitro*, they reported that this effect correlates with the ability of AVR3a to stabilize the host ubiquitin ligase CMPG1 (5).

Ellis and Dodds (13) highlighted the urgent need to test the requirement of PIP binding for effector uptake by host cells. Indeed, despite good structural models and extensive information about the biological effects of various mutations within the AVR3a protein effector domain, negligible data are available describing the influence of the R*x*LR leader on protein stability and dynamics. Here, we evaluated the effect that the R*x*LR leader exerts on the dynamics of the protein using recombinant protein constructs, and we describe an in-depth analysis of the lipid-binding properties of AVR3a. In addition, we analyzed the effect of a mutation within the AVR3a R*x*LR motif previously shown to prevent protein translocation into host cells, and we found that it impaired homodimerization of this effector.

[3] The abbreviations used are: PLP, phospholipid; GdnHCl, guanidine hydrochloride; AUC, analytical ultracentrifugation; ITC, isothermal titration calorimetry; PI3P, phosphoinositol 3-phosphate; Ins-1,3-P_2, inositol 1,3-bisphosphate.

MATERIALS AND METHODS

Detailed descriptions of all methods are given under supplemental "Materials and Methods."

Isothermal Titration Calorimetry—Titration experiments were performed with a MicroCal ITC$_{200}$ system at 20 °C. Titrant stock solutions were always prepared with the same batch of buffer as used for dialysis. Since the initial injection generally delivers inaccurate data, the first step was omitted from the analysis. The collected data were analyzed with the program Origin (MicroCal) using the binding models provided by the supplier. Errors correspond to the S.D. of the nonlinear least-squares fit of the data points of the titration curve.

PLP Binding—The lipid spot membranes were equilibrated for 10 min with PBS containing 0.1% Tween 20 and 5% lipid-free BSA before adding the respective protein constructs. Protein incubations were carried out for 20 min at room temperature. Subsequently, the membranes were extensively washed with PBS/Tween/BSA. Antibody detection was performed with a HRP-coupled anti-His antibody in PBS/Tween/BSA at a titer of 1:10,000 using ECL.

Lipid Binding under Denaturing Conditions—The membranes where equilibrated in PBS containing 0.1% Tween 20, 5% lipid-free BSA, and 8 M urea or 6 M guanidine hydrochloride (GdnHCl). The protein was pre-equilibrated in the same buffer for 30 min before addition to the membranes. After incubation, the membranes were extensively washed with PBS/Tween containing 8 M urea or 6 M GdnHCl, respectively, and re-equilibrated with PBS/Tween.

Circular Dichroism Spectra—These were recorded on a Jasco J-710 instrument in 50 mM degassed sodium phosphate buffer. Before recording the CD spectra used to determine the urea transition of AVR3a(22–147)-His$_6$, the protein was diluted into buffer containing the indicated urea concentration.

Formaldehyde Cross-linking—This was carried out for 5 min with 20 μM protein and 2% formaldehyde in 50 mM sodium phosphate buffer. The reaction was stopped by addition of an equal volume of Laemmli SDS sample buffer containing 2% β-mercaptoethanol and boiling for 10 min at 95 °C.

Analytical Ultracentrifugation—Analytical ultracentrifugation (AUC) experiments were carried out on a Beckman XL-I analytical ultracentrifuge with an An-50 Ti rotor. The sedimentation velocity experiments were performed in double-sector Epon charcoal-filled centerpieces at 4 °C at a speed of 45,000 rpm. Absorbance measurements were recorded at 280 and 220 nm. Exactly 200 scans of each cell were taken in continuous mode at 2-min intervals with a step size of 0.003 cm over a duration of ~17 h. The data were fitted to a model using the software SEDFIT and SEDNTERP. For calculation of the dimerization constants, global analysis using monomer-dimer or monomer-*n*-mer self-association models was performed for each sample with the data collected at three different concentrations. Errors in the binding constants were calculated by *F*-statistics analysis.

RESULTS

Rationales for AVR3a Construct Design—To gain insight into the function of the AVR3a R*x*LR leader, three different

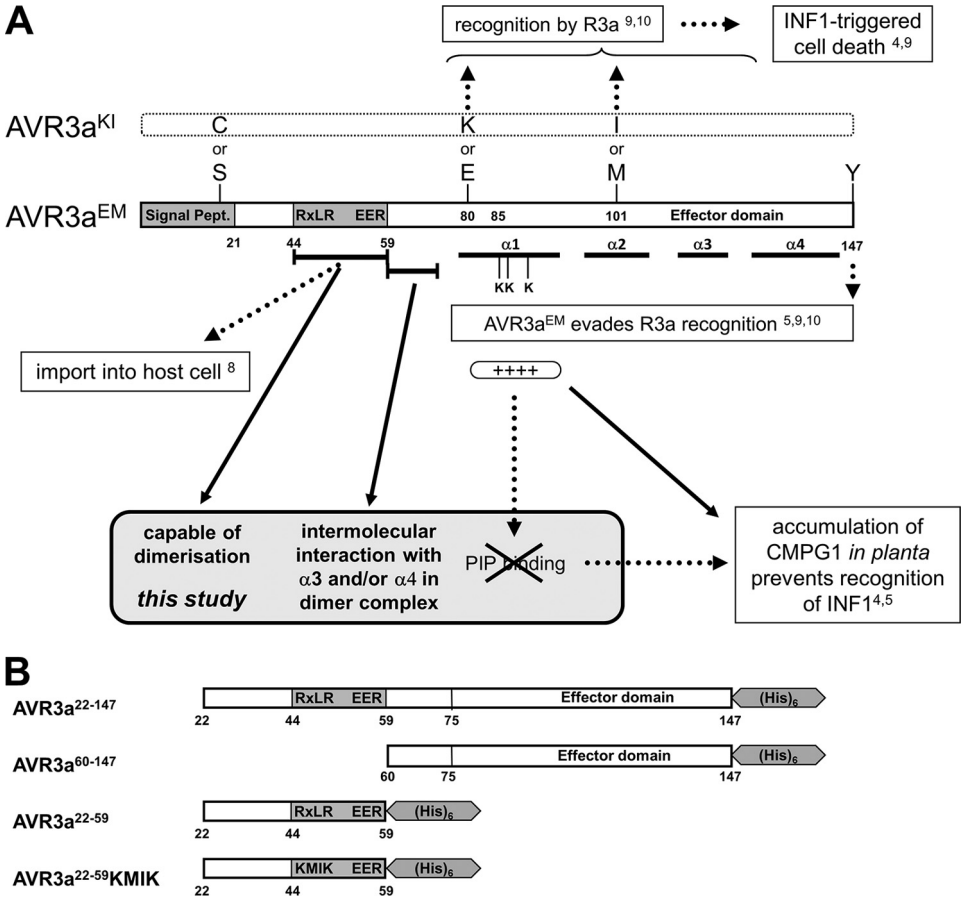

SCHEME 1. *A*, schematic summary of the currently published literature on AVR3a. *Dotted arrows* highlight the conclusions of the cited references, and the *solid arrows* indicate the suggested additions/modifications based on the data presented here. *B*, schematic representations of the AVR3a constructs investigated in this work.

$AVR3a^{KI}$ protein fragments were studied (Scheme 1*B*). The AVR3a fragment comprising amino acids 22–147 lacked only the signal peptide that is expected to be missing in the mature protein. For the AVR3a effector domain construct, residues 60–147 were chosen because this sequence has the same R3a recognition potential *in planta* as residues 22–147 (10). The R*x*LR leader construct comprised only amino acids 22–59. This exact sequence was previously shown to be important for the delivery of AVR3a by *P. infestans* into host cells (8) and does not affect the *in planta* recognition by R3a (10). Furthermore, a protein was produced in *Escherichia coli* in which the AVR3a R*x*LR motif was mutated, AVR3a(22–59)-His_6-KMIK. This mutant was found to impair the delivery of the full-length protein from the pathogen into host cells (8). All AVR3a fragments were fused to the His_6 tag of pET21b at the C terminus and were characterized in detail prior to use (supplemental Fig. S1 and Note 1).

N-terminal RxLR Leader of AVR3a Mediates Dimerization of the Protein in Vitro—Size exclusion chromatograms revealed a significant difference in the chromatogram of AVR3a(60–147)-His_6 compared with that of AVR3a(22–147)-His_6 (Fig. 1*A*). The apparent molecular mass calculated for AVR3a(22–147)-His_6 (see supplemental Fig. S2 for additional information) showed that this construct corresponded to that of a dimeric protein, whereas AVR3a(60–147)-His_6, in which the R*x*LR leader was deleted, behaved like a monomer. Under the same conditions, the AVR3a R*x*LR leader construct, AVR3a(22–59)-His_6, showed three peaks corresponding to a tetramer, dimer, and monomer, with the dimer as the dominant species (Fig. 1*B* and supplemental Fig. S2*A*).

To confirm these findings at lower, biologically more relevant concentrations, all constructs that showed dimerization were evaluated by AUC. AUC monitors the sedimentation of macromolecules in solution, which allows the characterization of protein oligomers. Each protein sample was analyzed at different concentrations, and the data were combined to calculate the respective dissociation constants (K_D). Consistent with the gel filtration results, AVR3a(22–147)-His_6 was identified as a homodimer. The K_D determined for the AVR3a(22–147)-His_6 dimerization was 10.83 ± 1.8 μM, which nearly matched the K_D obtained for the R*x*LR-only construct, AVR3a(22–59)-His_6 (9.8 ± 1.45 μM) (Fig. 1*C* and supplemental Appendix 1). For both constructs, the dimer concentrations were inversely proportional to the protein concentration under these conditions.

The K_D dimerization constant of AVR3a(22–147)-His_6 also coincided with the concentration that resulted in a half-maximal drop in the melting temperature (T_m) that was observed when the thermostability of the protein was characterized in a concentration-dependent manner (supplemental Fig. S3). A T_m difference of ~12 °C was observed when the heat denaturation of low concentration solutions was compared with that of high concentration solutions. The concentration obtained that cor-

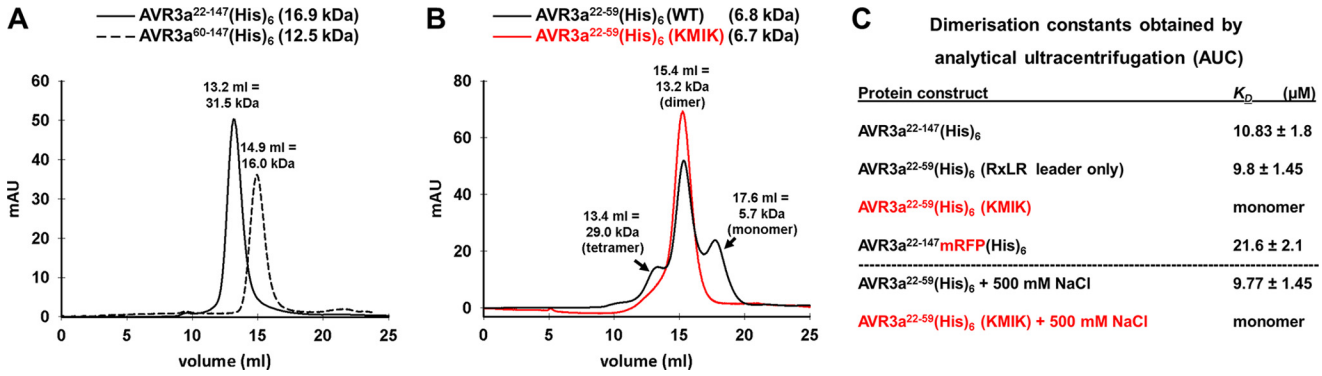

C

Dimerisation constants obtained by analytical ultracentrifugation (AUC)

Protein construct	K_D (μM)
AVR3a$^{22-147}$(His)$_6$	10.83 ± 1.8
AVR3a$^{22-59}$(His)$_6$ (RxLR leader only)	9.8 ± 1.45
AVR3a$^{22-59}$(His)$_6$ (KMIK)	monomer
AVR3a$^{22-147}$mRFP(His)$_6$	21.6 ± 2.1
AVR3a$^{22-59}$(His)$_6$ + 500 mM NaCl	9.77 ± 1.45
AVR3a$^{22-59}$(His)$_6$ (KMIK) + 500 mM NaCl	monomer

FIGURE 1. **RxLR leader of AVR3a promotes dimerization of the protein *in vitro*.** *A*, the size exclusion profile of AVR3a(22–147)-His$_6$ (500 μl of 259 μM loaded; *solid line*) revealed a dimeric protein, whereas AVR3a(60–147)-His$_6$ (500 μl of 187 μM loaded; *dashed line*) was found to be a monomer. *mAU*, milli-absorbance units. *B*, gel filtration run profiles of AVR3a(22–59)-His$_6$ (500 μl of 811 μM loaded; *black line*) and AVR3a(22–59)-His$_6$-KMIK (500 μl of 652 μM loaded; *red line*). AVR3a(22–59)-His$_6$ showed an equilibrium between a tetramer, dimer, and monomer, with the dimer form as the dominant species. The gel filtration chromatogram of AVR3a(22–59)-His$_6$-KMIK showed a peak retention corresponding to a dimer form. *C*, K_D values for the dimer formation for the indicated proteins obtained by AUC.

responded to $T_{m(½)}$ was ~15 μM. This shows that AVR3a(22–147)-His$_6$ is slightly more (thermo)stable at low concentrations. In contrast to the gel filtration runs, no tetrameric species for AVR3a(22–59)-His$_6$ were observed with AUC. Overall, these observations show that, *in vitro*, AVR3a is an oligomeric protein, principally a homodimer, and that dimerization is facilitated by the R*x*LR leader region.

To evaluate the effect that the C-terminal His$_6$ tag fusions might have on the dimerization constants of AVR3a, amino acids 22–147 were C-terminally fused with monomeric red fluorescent protein, a protein roughly double the size of AVR3a, and analyzed by AUC. A fluorescent reporter protein was chosen because these are commonly used to study protein localization and/or trafficking. This bulky fusion construct, AVR3a(22–147)-monomeric red fluorescent protein-His$_6$, showed only a slightly increased dimerization constant of 21.6 ± 2.1 μM (Fig. 1*C* and supplemental Appendix 1). Therefore, we expect that the C-terminal His$_6$ tag only marginally decreases the dimerization of AVR3a.

Mutations of RxLR Amino Acids RRLLR to KKMIK Leads to Structural Changes in the Leader and Inhibits Dimerization of AVR3a—The homologous replacement of the RRLLR sequence in AVR3a to KKMIK was shown to abolish AVR3a delivery by the pathogen to potato host cells (8). CD spectroscopic comparison of the AVR3a(22–59)-His$_6$ WT R*x*LR leader peptide and the AVR3a(22–59)-His$_6$-KMIK mutant peptide revealed that this mutation decreased the content of random coil structure and/or structural flexibility (supplemental Fig. S8*A*; see also supplemental Note 1 for further information).

The gel filtration chromatogram of AVR3a(22–59)-His$_6$-KMIK indicated that this polypeptide adopted a dimer form at high concentrations (652 μM) (Fig. 1*B* and supplemental Fig. S2*A*). However, subsequent analysis by AUC revealed only sedimentation coefficients consistent with a monomeric polypeptide at all protein concentrations tested (37, 74, and 111 μM) (Fig. 1*C* and supplemental Appendix 1). A control experiment showed that this discrepancy could not be ascribed to an ionic strength effect of the 500 mM NaCl used in the size exclusion chromatography buffer (Fig. 1*C*, *last two rows*, and supplemental Appendix 1). In the presence of 500 mM NaCl and at all tested concentrations (37, 74, and 111 μM), only monomeric species were detected for AVR3a(22–59)-His$_6$-KMIK. Therefore, we attribute the discrepancy for AVR3a(22–59)-His$_6$-KMIK to the difference in the protein concentrations utilized by AUC and gel exclusion. Due to the low extinction coefficient of the R*x*LR leader constructs at 280 nm (2980 M^{-1} cm^{-1}), high protein concentrations (600–800 μM) were required to obtain good quality gel filtration chromatograms.

We conclude that the AVR3a(22–59)-His$_6$-KMIK homodimer forms only at concentrations that exceed those utilized for AUC (111 μM). Therefore, this mutant construct is most likely a monomer at biologically relevant concentrations.

RxLR Leader of AVR3a Facilitates Intermolecular Dimerization with the Predicted α-Helix 3 and/or α-Helix 4—To further analyze the dimerization of AVR3a, cross-linking experiments were performed using formaldehyde. At ambient temperature, formaldehyde forms predominantly immonium cations that are reactive toward nucleophiles, such as the N terminus of a protein and the lateral chains of cysteine, lysine, histidine, and tyrosine residues (14). Formaldehyde is ideal to detect specific protein-protein interactions due to (i) a short reaction time that minimizes nonspecific cross-linking, (ii) the formation of highly reactive intermediates that allow fixation of transient interactions, and (iii) a short cross-linking distance (~0.2–0.3 nm) (15). Cross-linking conditions were optimized for AVR3a(22–147)-His$_6$ at room temperature. However, we noted that formaldehyde treatment reduced the efficiency of His tag detection by Western blotting. Therefore, all Western blots were slightly overexposed to visualize effects better. The example shown in Fig. 2 is representative for all experiments performed.

The different AVR3a constructs were cross-linked at concentrations of 20 μM alone and in combination with one another. Subsequently, the samples were analyzed by SDS-PAGE/Western blotting and compared with the untreated controls. Cross-linking of AVR3a(22–59)-His$_6$ (R*x*LR leader only) did not yield detectable amounts of covalently linked dimers (Fig. 2, *lanes 1* and *2*). Therefore, none of the lysines, tyrosines, and histidines (cysteine not present), highlighted in the sequence alignment in supplemental Fig. S4, are within 0.2–0.3

	M_W	1	2	3	4	5	6	7	8	9	10	11	12
AVR3a$^{22-59}$(His)$_6$	6.8kDa	x	x			x							x
AVR3a$^{22-147}$(His)$_6$	16kDa			x	x	x			x			x	
AVR3a$^{22-59}$(His)$_6$ (KMIK)	6.7kDa						x	x	x				
AVR3a$^{60-147}$(His)$_6$	12kDa									x	x	x	x
Formaldehyde	------		x		x	x		x	x		x	x	x

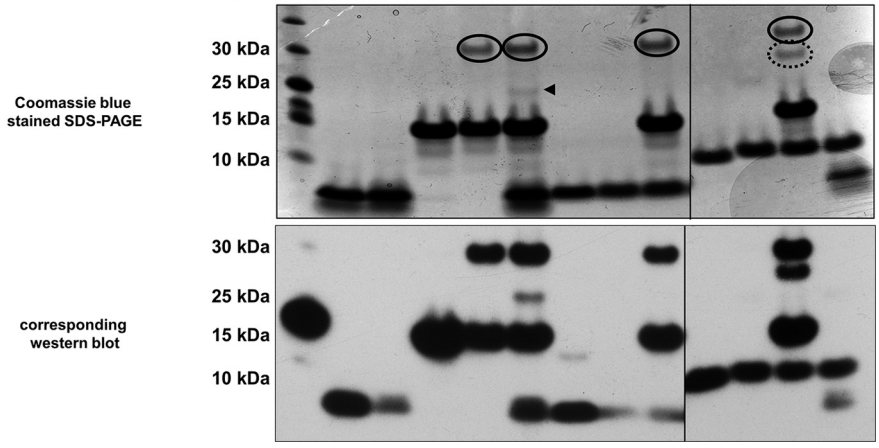

FIGURE 2. **Detection of AVR3a dimer complexes after formaldehyde cross-linking.** Cross-linking was carried out using 2% formaldehyde with the indicated proteins at a concentration of 20 μM in 50 mM sodium phosphate buffer (pH 7.2) for 5 min. Compared with untreated controls, no additional bands for the dimeric polypeptide AVR3a(22–59)-His$_6$ (*lanes 1* and *2*) were detected after formaldehyde treatment, indicating that no Lys, Tyr, or His is a 2–3-Å distance to one another in the dimer complex. The same was found for AVR3a(22–59)-His$_6$-KMIK, which was exclusively a monomer at a concentration of 20 μM (*lanes 6* and *7*). Formaldehyde treatment of AVR3a(22–147)-His$_6$ led to the appearance of a new band (*full ovals*) on the SDS-polyacrylamide gel, consistent with the dimeric size of the protein (*lanes 3* and *4*). When cross-linking of AVR3a(22–147)-His$_6$ was carried out in the presence of the AVR3a R*x*LR leader construct (AVR3a(22–59)-His$_6$), a new protein band appeared (*lane 5*, *arrowhead*), in addition to the AVR3a(22–147)-His$_6$ dimer complex. The size corresponded to a complex of both proteins, which could not be detected when AVR3a(22–59)-His$_6$ was substituted with AVR3a(22–59)-His$_6$-KMIK (*lane 8*). The AVR3a(60–147)-His$_6$ monomeric protein did not cross-link to itself with formaldehyde (*lanes 9* and *10*). Surprisingly, AVR3a(60–147)-His$_6$ could be cross-linked to AVR3a(22–147)-His$_6$ (*lane 11*, *dotted oval*) but not to AVR3a(22–59)-His$_6$ (*lane 12*). See supplemental Appendix 3 for further information.

nm of one another in the dimer complexes. In contrast, formaldehyde treatment of AVR3a(22–147)-His$_6$ led to covalent cross-linked dimers (Fig. 2, *lanes 3* and *4*). Furthermore, AVR3a(22–59)-His$_6$ could be successfully cross-linked to AVR3a(22–147)-His$_6$ (Fig. 2, *lane 5*). Surprisingly, a covalently linked mixed dimer complex was clearly detected when AVR3a(60–147)-His$_6$ was cross-linked in the presence of AVR3a(22–147)-His$_6$ (Fig. 2, *lane 11*). However, no cross-linked product was found after formaldehyde treatment of AVR3a(60–147)-His$_6$ alone (Fig. 2, *lanes 9* and *10*) or when co-incubated with AVR3a(22–59)-His$_6$ (*lane 12*). These observations show that the AVR3a dimerization is not strictly dependent on the R*x*LR leader (residues 22–59) but requires additional sequence elements. The successful cross-linking of AVR3a(22–147)-His$_6$ to AVR3a(60–147)-His$_6$ indicates an intermolecular interaction of the R*x*LR leader with the effector domain. In addition, no covalent species were observed when AVR3a(22–59)-His$_6$-KMIK was probed for its ability to cross-link to the full-length AVR3a construct (amino acids 22–147) (Fig. 2, *lane 8*). These results are consistent with the observation made by AUC that this polypeptide was unable to form a dimer at a concentration of 20 μM (see supplemental Note 2 for further information).

To further characterize the AVR3a dimerization, samples of the monomer and dimer bands of AVR3a(22–147)-His$_6$ were cut from the gel, digested with trypsin, separated by liquid chromatography, and subsequently analyzed by MALDI-TOF mass spectrometry (supplemental Appendix 2). The chromatograms were very similar for both the dimer and monomer samples, with the exception of one distinct peak that appeared only in the dimer sample. MALDI-TOF lift experiments revealed peptides covering AVR3a amino acids 59–79 (APNFNLASLNEEMFNVAALTK); these amino acids are located C-terminal after the EER motif, including the beginning of the predicted helix α1, amino acids 110–120 (VTLDQIDTFLK), nearly the complete predicted α-helix 3, amino acids 131–147 (YNQIYNSYMMHLGLTGY), and the predicted α-helix 4 (AVR3a helix prediction according to Ref. 4). In addition, a partial proteolytic digest of AVR3a(22–147)-His$_6$ was performed to identify the possible starting point of the AVR3a effector domain (supplemental Fig. S5). This experiment showed a proteinase K-resistant C-terminal domain starting at amino acid 68. Therefore, we conclude that AVR3a residues 59–68 are located close to the effector domain of the partner molecule in the tertiary dimer complex.

Lipid-binding Property of the AVR3a Effector Domain Results from a Denatured Protein Fraction—Since PLP binding of oomycete R*x*LR effectors is currently controversial (13), we investigated the lipid-binding ability of AVR3a using lipid spot membranes. We first confirmed the observations made by Yaeno *et al.* (4) that indeed the effector domain and not the R*x*LR leader of AVR3a binds membrane-attached PLPs (Fig. 3*A*). As already underlined by these authors, this result is in contrast with a previous report claiming that the interaction of oomycete R*x*LR proteins with PLPs is attributed to the R*x*LR leader (motif) (10).

To investigate the possible physiological significance of PLP binding, experiments were performed utilizing denatured

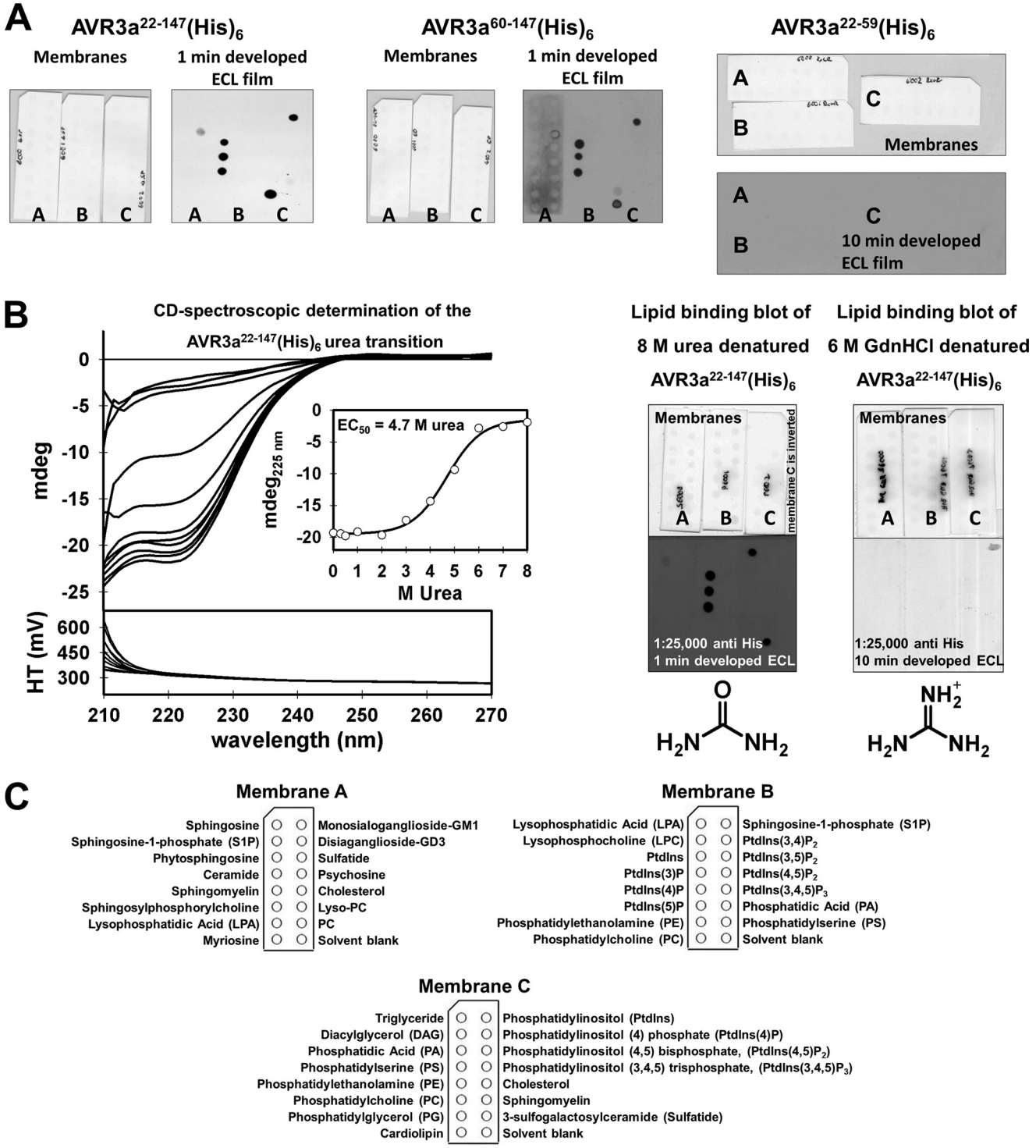

FIGURE 3. **Lipid binding of AVR3a does not require an intact structure.** *A*, the full-length AVR3a protein construct (AVR3a(22–147)-His_6) and the RxLR leader truncated construct AVR3a(60–147)-His_6 were able to bind to PLPs on lipid spot membranes. No lipid binding could be detected for the RxLR leader construct. The membranes were incubated for 20 min with 20 μM protein. The lipid recognized on *membrane A* was sulfatide; those on *membrane B* were phosphatidylinositol 3-, phosphatidylinositol 4-, and phosphatidylinositol 5-phosphate; and those on *membrane C* were phosphatidylglycerol, cardiolipin, and phosphatidylinositol 4-phosphate. *B*, urea- but not guanidine-denatured AVR3a(22–147)-His_6 binds to PLPs. The urea transition of 5 μM AVR3a(22–147)-His_6 was measured using CD spectroscopy. The urea transition point was 4.68 M. To analyze the lipid-binding ability of unfolded AVR3a(22–147)-His_6, the lipid binding assay was performed in the presence of 8 M urea and 6 M GdnHCl, respectively. No difference in the lipid binding of native and urea-denatured AVR3a(22–147)-His_6 could be found, whereas the presence of a 6 M concentration of the charged chemical denaturant GdnHCl completely abolished the lipid binding of AVR3a(22–147)-His_6. *mdeg*, millidegrees; *HT*, high tension voltage. *C*, identity of the lipids found on the spot membrane.

AVR3a(22–147)-His_6. The urea transition of AVR3a(22–147)-His_6 was measured by following the loss of secondary structure with increased urea concentrations using CD spectroscopy. The urea EC_{50} is 4.7 M (Fig. 3*B*), and the protein is completely unfolded at concentrations above 6 M. Surprisingly, when the PLP binding assay was performed in the presence of 8 M urea,

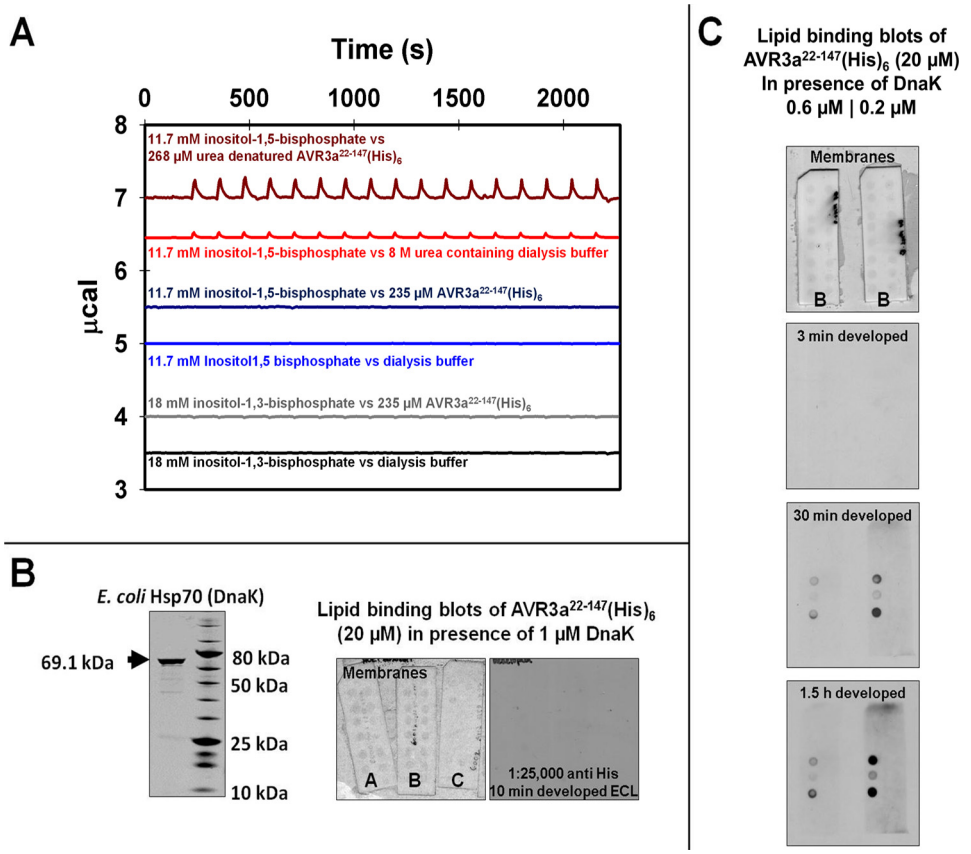

FIGURE 4. **Lipid binding of the AVR3a effector domain is attributable to a small proportion of denatured molecules.** *A*, native AVR3a(22–147)-His_6 did not bind Ins-1,3-P_2 or Ins-1,5-P_2, the polar headgroups of phosphatidylinositol 3- and phosphatidylinositol 5-phosphate, respectively. No difference between a titration of 18 mM Ins-1,3-P_2 into the dialysis buffer (*black traces*) and buffer containing 235 μM AVR3a(22–147)-His_6 (*gray traces*) was found. The same was observed for titrations utilizing 11.7 mM Ins-1,5-P_2 (*blue* and *dark blue traces*). The dialysis buffer used to dissolve the titrants was 50 mM sodium phosphate (pH 7.2). The thermogram recorded for the titration of Ins-1,5-P_2 (11.7 mM) to 8 M urea-denatured AVR3a(22–147)-His_6 (268 μM) indicates a weak interaction between both molecules under these conditions (*red* and *dark red traces*). However, the thermograms show that the stoichiometry was greater than 1:8 (concentration range covered by the titration) because there is no obvious enthalpy change visible in the titration profile. In addition, the binding constant (K_D) must be >1.92 mM. The dialysis buffer for this type of experiment was 50 mM sodium phosphate (pH 7.2) containing 8 M urea. All titrations were carried out at 20 °C. *B*, lipid binding of AVR3a(22–147)-His_6 was abolished in presence of substoichiometric amounts of the *E. coli* Hsp70 chaperone DnaK. Lipid binding of 20 μM AVR3a(22–147)-His_6 to lipids on lipid spot membranes was suppressed by the presence of ADP-bound DnaK at a molar concentration (1 μM) that represents 5% of the AVR3a(22–147)-His_6 amount. *C*, lipid binding of 20 μM AVR3a(22–147)-His_6 in the presence of DnaK amounts corresponding to 3% (0.6 μM) and 1% (0.2 μM) of the AVR3a(22–147)-His_6 molar concentration. Lipid spot identity can be found in Fig. 3*C*.

we found that denatured AVR3a(22–147)-His_6 interacted with PLPs with the same specificity as the non-denatured protein solutions (Fig. 3*B*). In contrast, no PLP binding of AVR3a(22–147)-His_6 was detectable when the assay was carried out with a 6 M concentration of the charged chemical denaturant GdnHCl instead of urea (Fig. 3*B*). These observations demonstrate that PLP binding of AVR3a does not require an intact three-dimensional structure, that it is likely based on charge-charge interactions, and that the headgroups of the recognized PLPs are mainly responsible for this interaction. Thus, we characterized this binding by isothermal titration calorimetry (ITC) utilizing both native and urea-denatured AVR3a(22–147)-His_6 as baits. As a titrant, we chose the phosphoinositol 3-phosphate (PI3P) headgroup, inositol 1,3-bisphosphate (Ins-1,3-P_2), because this PLP was reported to be the main component responsible for R*x*LR protein translocation (11). We also utilized the phosphoinositol 5-phosphate headgroup, Ins-1,5-P_2, because this PLP was reported to have the highest binding affinity on lipid spot membranes for the AVR3a effector domain (4). Surprisingly, no change in enthalpy was detected in the titrations with either Ins-1,3-P_2 or Ins-1,5-P_2 using native AVR3a(22–147)-His_6 as a bait even at high, biologically irrelevant concentrations (Fig. 4*A*). To ensure that an eventual positively charged PLP-binding surface of AVR3a(22–147)-His_6 was not obscured through the presence of phosphate ions, a control titration with Ins-1,3-P_2 was performed in the absence of phosphate buffer. Again, no difference between the buffer control titration and the experiment containing AVR3a(22–147)-His_6 as a bait could be observed (supplemental Fig. S6).

Since charge-charge dominated protein-ligand interactions are normally characterized by endothermic ITC profiles (16), the actual amount of complex detected in the membrane assay had to be below the detection limit of ITC. This suggested that a small fraction of unfolded AVR3a(22–147)-His_6 molecules might bind to the PLPs. To test this hypothesis, ITC titrations utilizing Ins-1,5-P_2 and AVR3a(22–147)-His_6 were performed in the presence of 8 M urea. The thermograms show signals indicative of nonspecific interactions, and only a marginal change in enthalpy could be observed within the investigated concentration range (Fig. 4*A*).

These experiments show that the binding stoichiometry must be above 1:8 (concentration range covered by the titra-

tions) and that the binding constant has to exceed the final ligand concentration of 1.92 mM. Therefore, it should be possible to block the observed lipid binding of AVR3a(22–147)-His_6 on spot membranes with substoichiometric amounts of a chaperone that specifically binds unfolded protein molecules. To test this, we utilized the *E. coli* chaperone DnaK. DnaK was purified in the absence of its co-chaperones DnaJ (the DnaK hydrolysis factor) and GrpE (the nucleotide exchange factor) in an ADP-bound state, also referred to as the high affinity state (17–21). In this form, DnaK binds proteins that expose hydrophobic surface patches. The ADP-DnaK-unfolded protein complexes usually have dissociation half-times of minutes to even hours (17). Thus, a nearly 1:1 binding of DnaK to misfolded AVR3a(22–147)-His_6 can be assumed during the 20-min incubation time of the performed lipid spot assay. No AVR3a(22–147)-His_6 could be immunodetected on the lipid spot membranes following co-incubation of 20 μM AVR3a(22–147)-His_6 and 1 μM DnaK, even after prolonged film exposure (Fig. 4, *B* and *C*). This demonstrates that <5% of the AVR3a molecules are able to bind to the PLPs and that either no or only a very slow transition toward a lipid-binding conformational state exists in AVR3a(22–147)-His_6 molecules.

To investigate the binding to PLPs presented in a more natural context, AVR3a(22–147)-His_6 was probed for its ability to bind PolyPIPosomes in different buffers (supplemental Fig. S10). Consistent with the lipid spot membrane experiments, AVR3a(22–147)-His_6 was found to bind PI3P-containing PolyPIPosomes when denatured with 8 M urea and in the absence of the stabilizing ions phosphate and/or sulfate. To evaluate the competition effect of phosphate ions on PI3P binding, we tested the p40 PX-binding domain in the presence and absence of these. 50 mM sodium phosphate buffer slightly inhibited the PI3P-p40 PX binding, but the interaction could still be clearly detected (supplemental Fig. S10, *lower*). These observations confirm that denatured AVR3a(22–147)-His_6 has an affinity for PI3P and that phosphate and/or sulfate ions are crucial for structural stabilization of this protein construct.

DISCUSSION

Protein self-association to form dimers is widely found in biology (22). We have shown here that recombinant AVR3a forms a homodimer *in vitro* (Figs. 1 and 2). Its dissociation constant is ~10 μM, a value often found in other homodimers (for examples, see Refs. 23–25). Dimerization of AVR3a is mainly (but not solely) facilitated by the R*x*LR leader because the recombinant protein comprising these residues exhibited the same K_D as the full-length protein (Fig. 1 and supplemental Appendix 1). In addition, the dimerization constant of the AVR3a R*x*LR leader is independent of the solvent ionic strength (Fig. 1*C* and supplemental Appendix 1), suggesting that this complex formation is not driven by charge-charge interactions. Interestingly, the authors of a recent study tested whether AVR3a dimerizes *in planta* (26). For this purpose, the authors coexpressed two different N-terminally tagged (FLAG and GFP) AVR3a constructs *in planta* but were unable to detect any interaction between these two proteins in co-immunoprecipitation experiments. However, this finding does not necessarily mean that the dimer form of AVR3a is biologically irrelevant. It still could play a role during trafficking and secretion from the parasite or during translocation into the host cells. In addition, here we studied solely C-terminally tagged recombinant constructs to investigate the role that the N-terminal R*x*LR leader plays for the protein because direct addition of a tag to a sequence of interest can alter the biological function of the respective polypeptide (see review, see Ref. 27). We found that a C-terminal extension to AVR3a of ~28 kDa still allowed dimerization but also slightly reduced the respective K_D value. It is possible that N-terminal tags more strongly affect the structure and dynamics of the short and flexible AVR3a R*x*LR leader because we found that parts of the R*x*LR leader are in 2–3-Å contact with some amino acids of the effector domain (Fig. 2 and supplemental Appendix 2). We are aware that those studying the effects that AVR3a facilitates on the host prefer detectable modifications on the N terminus of the protein because a free C terminus is crucial for the suppression of the plant immune defense response against INF1 (4, 5, 10). Nevertheless, on the basis of our findings, we believe that the biological significance of AVR3a dimerization should best be investigated with constructs containing small C-terminal tags.

In addition, we investigated a previously described mutation of the R*x*LR amino acids within the leader of AVR3a (residues 43–47, RRLLR changed to KKMIK) (8). Interestingly, this mutation altered the secondary structure ensemble of the R*x*LR leader (supplemental Fig. S7*A*), and the respective polypeptide showed at least a 10-fold increased dimerization constant *in vitro* (Fig. 1, *B* and *C*, and supplemental Appendix 1). Furthermore, the mutation reduced the ability of the R*x*LR leader peptide to interact with full-length AVR3a (Fig. 2 and supplemental Fig. S7, *B* and *C*, and Note 2). Since the investigated mutant showed strongly altered characteristics compared with the WT, we believe that the biologically observable effects of R*x*LR motif mutations require *in vitro* characterization of the respective mutants to better understand the nature of the observed effects.

Several recent publications reported that some oomycete and fungal effectors interact with the headgroups of phosphoinositol monophosphates (4, 11, 12, 28). In addition, claims were made that, for oomycete R*x*LR proteins, R*x*LR or R*x*LR-like motifs in their respective N-terminal regions facilitate pathogen-independent translocation through binding to cell surface-exposed PI3P (11, 28). This view has been discussed (13) and challenged by two independent groups (4, 12). While studying the lipid binding of AVR3a, we found that the protein was indeed detectable by antibodies on certain matrix-associated PLPs. In addition, we could reproduce the findings by Yaeno *et al.* (4) that the C-terminal effector domain, not the R*x*LR leader of AVR3a, bound the PLPs. However, we found that this PLP-binding ability of AVR3a did not require an intact three-dimensional structure and that only a small subfraction of presumably misfolded molecules are responsible (Figs. 3 and 4 and supplemental Fig. S10). Furthermore, we were unable to detect any signs of a physical interaction between native AVR3a and the PLP headgroup Ins-1,3-P_2 or Ins-1,5-P_2 using ITC (Fig. 4*A*). Furthermore, AVR3a seems to only bind PI3P-containing PolyPIPosomes when denatured or not sufficiently stabilized (supplemental Fig. S10). Our data also suggest that either no or only a very slow equilibrium toward a lipid-binding conforma-

tion exists in native AVR3a. Therefore, we would question the biological relevance that PLP binding plays for AVR3a. As an alternative, we recently discovered that a putative R*x*LR-like effector protein from the fish pathogenic oomycete *Saprolegnia parasitica* is translocated into fish cells via binding to a receptor that is tyrosine *O*-sulfated (29). It will be interesting to investigate whether R*x*LR proteins from plant pathogenic oomycetes use a similar strategy to enter plant cells.

Acknowledgments—We thank Sharon Kelly for use of the CD spectrometer, Prof. Ian Booth for use of the ITC_{200} system, and Prof. Neil A. R. Gow for helpful suggestions and discussions.

REFERENCES

1. Phillips, A. J., Anderson, V. L., Robertson, E. J., Secombes, C. J., and van West, P. (2008) New insights into animal pathogenic oomycetes. *Trends Microbiol.* **16,** 13–19
2. Gu, B., Kale, S. D., Wang, Q., Wang, D., Pan, Q., Cao, H., Meng, Y., Kang, Z., Tyler, B. M., and Shan, W. (2011) Rust secreted protein Ps87 is conserved in diverse fungal pathogens and contains an RXLR-like motif sufficient for translocation into plant cells. *PLoS ONE* **6,** e27217
3. Kale, S. D., and Tyler, B. M. (2011) Entry of oomycete and fungal effectors into plant and animal host cells. *Cell. Microbiol.* **13,** 1839–1848
4. Yaeno, T., Li, H., Chaparro-Garcia, A., Schornack, S., Koshiba, S., Watanabe, S., Kigawa, T., Kamoun, S., and Shirasu, K. (2011) Phosphatidylinositol monophosphate-binding interface in the oomycete RXLR effector AVR3a is required for its stability in host cells to modulate plant immunity. *Proc. Natl. Acad. Sci. U.S.A.* **108,** 14682–14687
5. Bos, J. I., Armstrong, M. R., Gilroy, E. M., Boevink, P. C., Hein, I., Taylor, R. M., Zhendong, T., Engelhardt, S., Vetukuri, R. R., Harrower, B., Dixelius, C., Bryan, G., Sadanandom, A., Whisson, S. C., Kamoun, S., and Birch, P. R. (2010) *Phytophthora infestans* effector AVR3a is essential for virulence and manipulates plant immunity by stabilizing host E3 ligase CMPG1. *Proc. Natl. Acad. Sci. U.S.A.* **107,** 9909–9914
6. Birch, P. R., Rehmany, A. P., Pritchard, L., Kamoun, S., and Beynon, J. L. (2006) Trafficking arms: oomycete effectors enter host plant cells. *Trends Microbiol.* **14,** 8–11
7. Rehmany, A. P., Gordon, A., Rose, L. E., Allen, R. L., Armstrong, M. R., Whisson, S. C., Kamoun, S., Tyler, B. M., Birch, P. R., and Beynon, J. L. (2005) Differential recognition of highly divergent downy mildew avirulence gene alleles by *RPP1* resistance genes from two *Arabidopsis* lines. *Plant Cell* **17,** 1839–1850
8. Whisson, S. C., Boevink, P. C., Moleleki, L., Avrova, A. O., Morales, J. G., Gilroy, E. M., Armstrong, M. R., Grouffaud, S., van West, P., Chapman, S., Hein, I., Toth, I. K., Pritchard, L., and Birch, P. R. (2007) A translocation signal for delivery of oomycete effector proteins into host plant cells. *Nature* **450,** 115–118
9. Armstrong, M. R., Whisson, S. C., Pritchard, L., Bos, J. I., Venter, E., Avrova, A. O., Rehmany, A. P., Böhme, U., Brooks, K., Cherevach, I., Hamlin, N., White, B., Fraser, A., Lord, A., Quail, M. A., Churcher, C., Hall, N., Berriman, M., Huang, S., Kamoun, S., Beynon, J. L., and Birch, P. R. (2005) An ancestral oomycete locus contains late blight avirulence gene *Avr3a*, encoding a protein that is recognized in the host cytoplasm. *Proc. Natl. Acad. Sci. U.S.A.* **102,** 7766–7771
10. Bos, J. I., Kanneganti, T. D., Young, C., Cakir, C., Huitema, E., Win, J., Armstrong, M. R., Birch, P. R., and Kamoun, S. (2006) The C-terminal half of *Phytophthora infestans* RXLR effector AVR3a is sufficient to trigger R3a-mediated hypersensitivity and suppress INF1-induced cell death in *Nicotiana benthamiana*. *Plant J.* **48,** 165–176
11. Kale, S. D., Gu, B., Capelluto, D. G., Dou, D., Feldman, E., Rumore, A., Arredondo, F. D., Hanlon, R., Fudal, I., Rouxel, T., Lawrence, C. B., Shan, W., and Tyler, B. M. (2010) External lipid PI3P mediates entry of eukaryotic pathogen effectors into plant and animal host cells. *Cell* **142,** 284–295
12. Gan, P. H., Rafiqi, M., Ellis, J. G., Jones, D. A., Hardham, A. R., and Dodds, P. N. (2010) Lipid binding activities of flax rust AvrM and AvrL567 effectors. *Plant Signal. Behav.* **5,** 1272–1275
13. Ellis, J. G., and Dodds, P. N. (2011) Showdown at the RXLR motif: serious differences of opinion in how effector proteins from filamentous eukaryotic pathogens enter plant cells. *Proc. Natl. Acad. Sci. U.S.A.* **108,** 14381–14382
14. Toews, J., Rogalski, J. C., Clark, T. J., and Kast, J. (2008) Mass spectrometric identification of formaldehyde-induced peptide modifications under *in vivo* protein cross-linking conditions. *Anal. Chim. Acta* **618,** 168–183
15. Sutherland, B. W., Toews, J., and Kast, J. (2008) Utility of formaldehyde cross-linking and mass spectrometry in the study of protein-protein interactions. *J. Mass Spectrom.* **43,** 699–715
16. Matulis, D., Rouzina, I., and Bloomfield, V. A. (2000) Thermodynamics of DNA binding and condensation: isothermal titration calorimetry and electrostatic mechanism. *J. Mol. Biol.* **296,** 1053–1063
17. Packschies, L., Theyssen, H., Buchberger, A., Bukau, B., Goody, R. S., and Reinstein, J. (1997) GrpE accelerates nucleotide exchange of the molecular chaperone DnaK with an associative displacement mechanism. *Biochemistry* **36,** 3417–3422
18. Slepenkov, S. V., and Witt, S. N. (2002) The unfolding story of the *Escherichia coli* Hsp70 DnaK: is DnaK a holdase or an unfoldase? *Mol. Microbiol.* **45,** 1197–1206
19. Russell, R., Jordan, R., and McMacken, R. (1998) Kinetic characterization of the ATPase cycle of the DnaK molecular chaperone. *Biochemistry* **37,** 596–607
20. Bukau, B., and Horwich, A. L. (1998) The Hsp70 and Hsp60 chaperone machines. *Cell* **92,** 351–366
21. Ellis, R. J., and Hartl, F. U. (1999) Principles of protein folding in the cellular environment. *Curr. Opin. Struct. Biol.* **9,** 102–110
22. Marianayagam, N. J., Sunde, M., and Matthews, J. M. (2004) The power of two: protein dimerization in biology. *Trends Biochem. Sci.* **29,** 618–625
23. Nickerson, D. P., and Wong, L. L. (1997) The dimerization of *Pseudomonas putida* cytochrome $P450_{cam}$: practical consequences and engineering of a monomeric enzyme. *Protein Eng.* **10,** 1357–1361
24. Burrows, S. D., Doyle, M. L., Murphy, K. P., Franklin, S. G., White, J. R., Brooks, I., McNulty, D. E., Scott, M. O., Knutson, J. R., and Porter, D. (1994) Determination of the monomer-dimer equilibrium of interleukin-8 reveals it is a monomer at physiological concentrations. *Biochemistry* **33,** 12741–12745
25. Phizicky, E. M., and Fields, S. (1995) Protein-protein interactions: methods for detection and analysis. *Microbiol. Rev.* **59,** 94–123
26. Boutemy, L. S., King, S. R., Win, J., Hughes, R. K., Clarke, T. A., Blumenschein, T. M., Kamoun, S., and Banfield, M. J. (2011) Structures of *Phytophthora* RXLR effector proteins. A conserved but adaptable fold underpins functional diversity. *J. Biol. Chem.* **286,** 35834–35842
27. Fidzinski, P., Wawra, M., Bartsch, J., Heinemann, U., and Behr, J. (2012) High-frequency stimulation of the temporoammonic pathway induces input-specific long-term potentiation in subicular bursting cells. *Brain Res.* **1430,** 1–7
28. Plett, J. M., Kemppainen, M., Kale, S. D., Kohler, A., Legué, V., Brun, A., Tyler, B. M., Pardo, A. G., and Martin, F. (2011) A secreted effector protein of *Laccaria* bicolor is required for symbiosis development. *Curr. Biol.* **21,** 1197–1203
29. Wawra, S., Bain, J., Durward, E., de Bruijn, I., Minor, K. L., Matena, A., Löbach, L., Whisson, S. C., Bayer, P., Porter, A. J., Birch, P. R., Secombes, C. J., and van West, P. (2012) Host-targeting protein 1 (SpHtp1) from the oomycete *Saprolegnia parasitica* translocates specifically into fish cells in a tyrosine *O*-sulfate-dependent manner. *Proc. Natl. Acad. Sci. U.S.A.* **109,** 2096–2101